Calibration Challenges for the Next Generation of Radio Telescopes

Stefan J. Wijnholds, Sebastiaan van der Tol, Ronald Nijboer and Alle-Jan van der Veen

Instruments for radio astronomical observations have come a long way. While the first telescopes were based on very large dishes and 2-antenna interferometers, current instruments consist of dozens of steerable dishes, whereas future instruments will be even larger distributed sensor arrays with a hierarchy of phased array elements. For such arrays to provide meaningful output (images), accurate calibration is of critical importance. Calibration must solve for the unknown antenna gains and phases, as well as the unknown atmospheric and ionospheric disturbances. Future telescopes will have a large number of elements and a large field of view. In this case the parameters are strongly direction dependent, resulting in a large number of unknown parameters even if appropriately constrained physical or phenomenological descriptions are used. This makes calibration a daunting parameter estimation task.

I. Introduction

Astronomers study the physical phenomena outside the Earth's atmosphere by observing cosmic particles and electromagnetic waves impinging on the Earth. Each type of observation provides another perspective on the universe thereby unraveling some mysteries while raising new questions. Over the years, astronomy has become a true multi-wavelength science. A nice demonstration is provided in Fig. 1. In this image, the neutral hydrogen gas observed with the Westerbork Synthesis Radio Telescope (WSRT) exhibits an intricate extended structure that is completely invisible in the optical image from the Sloan digital sky survey [1]. The radio observations therefore provide a radically different view on the dynamics of this galaxy.

Images like Fig. 1 are only possible if the instruments used to observe different parts of the electromagnetic spectrum provide a similar resolution. This poses quite a challenge since the resolution of any telescope is determined by the ratio of the wavelength and the telescope diameter. Consequently, the aperture of radio telescopes has to be 5 to 6 orders of magnitude larger than that of an optical telescope to provide comparable resolution, i.e. radio telescopes should have an aperture of several hundreds of kilometers. Although it is not feasible to make a dish of this size, it is possible to synthesize an aperture by building an interferometer, i.e., an array.

Radio astronomy started with the discovery by Karl Jansky, at Bell Telephone Laboratories in 1928, that the source of unwanted interference in his short-wave radio transmissions actually came from the Milky Way. For this, he used the large antenna mounted on a turntable shown in Fig. $2(a)$.

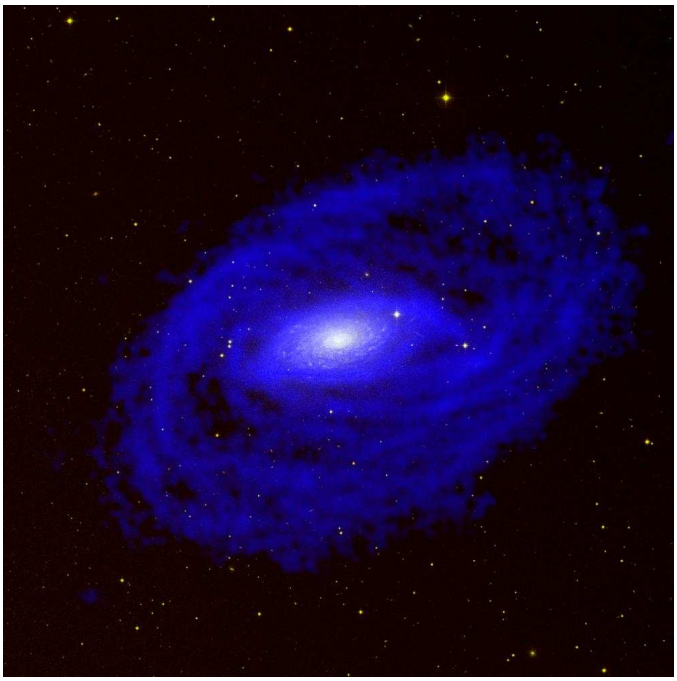

Fig. 1. Image of the spiral galaxy NGC 5055, showing the structure of the neutral hydrogen gas observed with the Westerbork Synthesis Radio Telescope (blue) superimposed on an optical image of the same galaxy from the Sloan digital sky survey (white) [2].

Subsequent single-antenna instruments were based on larger and larger dishes, culminating in the Arecibo telescope (Puerto Rico 1960, 305 m non-steerable dish) and the Effelsberg telescope (Bonn, Germany, 1972, 100 m steerable dish, Fig. $2(b)$). Making larger steerable dishes is not practical.

An interferometer measures the correlation between two antennas spaced at a certain distance. Initially used to study a single source passing over the sky, the principle was used in optical astronomy in the Michelson stellar interferometer (1890, 1920); the first radio observations using two dipoles were done by Ryle and Vonberg in 1946 [3]. Examples of subsequent instruments are: the Cambridge One Mile Telescope in Cambridge, UK (1964, 2 fixed and one movable 18.3 m dishes); the 3 km WSRT in Westerbork, The Netherlands (1970, 12 fixed and 2 movable 25 m dishes, Fig. $2(c)$); the 36 km Very Large Array (VLA) in Socorro, New Mexico, USA (1980, 27 movable 25 m dishes, Fig. $2(d)$); the 25 km Giant Meter-Wave Radio Telescope (GMRT) in Pune, India (1998, 30 dishes with 45 m diameter). These telescopes use the Earth rotation to obtain a sequence of correlations for varying antenna baseline orientations relative to the desired sky

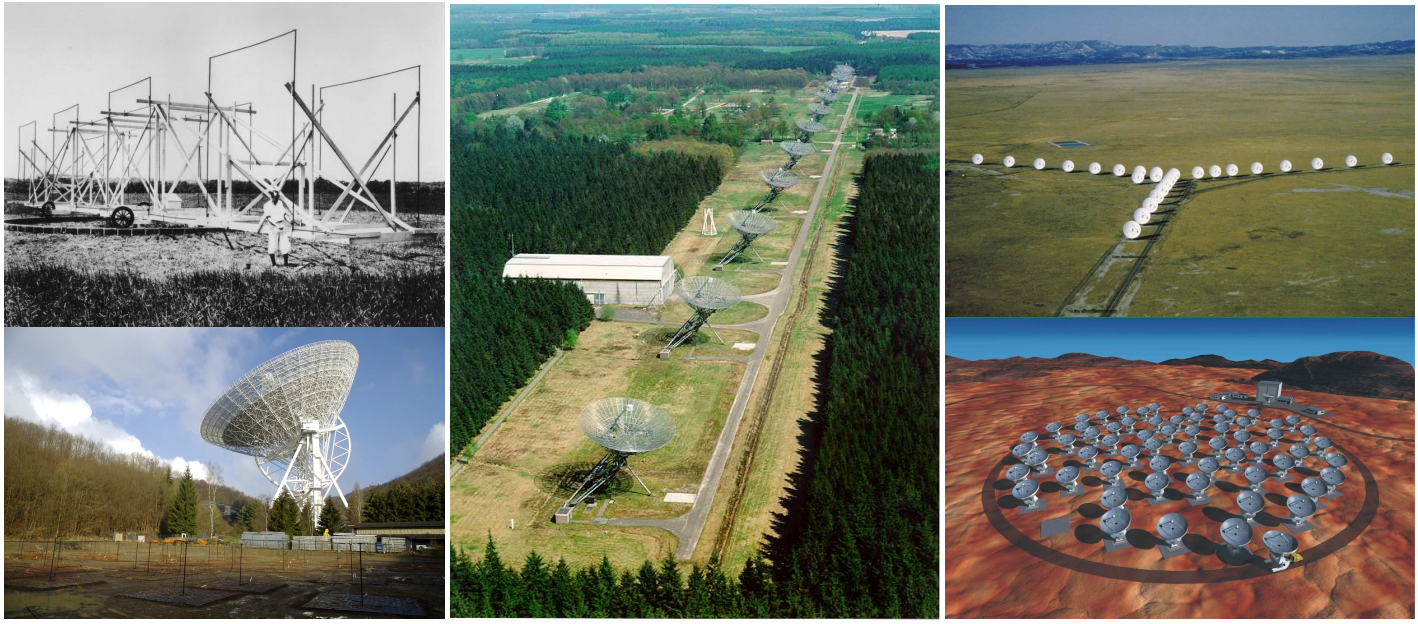

Fig. 2. The radio telescopes of (a) Jansky, (b) Effelsberg, (c) WSRT, (d) VLA, (e) concept for ALMA.

image field, resulting in high-resolution images via *synthesis mapping*. Even larger baselines (up to a few thousand km) were obtained by combining these instruments into a single instrument using a technique called VLBI (very long baseline interferometry), where the telescope outputs are time-stamped and post-processed by correlation at a central location. An extensive historical overview is presented in [4]. In the near future, astronomers are building even larger arrays, such as the Atacama Large Millimeter Array (ALMA, Chile, 2011, 50 movable 12 m dishes with possible extension to 64 dishes, Fig. 2(e)), the Low Frequency Array (LOFAR, The Netherlands (2009, about 30,000 dipole antennas grouped in 36 stations, Fig. 5), and the Square Kilometer Array (SKA, 2020+, Fig. 5). A recent issue of the Proceedings of the IEEE (Vol.97, No. 8, Aug. 2009) provides overview articles discussing many of the recent and future telescopes.

High-resolution synthesis imaging would not be possible without accurate calibration. Initially, the complex antenna gains and phases are unknown; they have to be estimated. Moreover, propagation through the atmosphere and ionosphere causes additional phase delays that may create severe distortions. Finally, image reconstruction or *map making* is governed by finite sample effects: we can only measure correlations on a small set of baselines. Solving for these three effects is intertwined and creates very interesting signal processing problems. In this overview paper, we focus on the calibration aspects, whereas imaging is covered in a companion paper [5]. The examples provided in this paper are generally borrowed from low frequency (< 1.5 GHz) instruments, but the framework presented is applicable to high frequency instruments like ALMA as well.

II. Interferometry and image formation

The concept of interferometry is illustrated in Fig. 3. An interferometer measures the spatial coherency of the incoming electromagnetic field. This is done by correlating the signals from the individual receivers with each other. The correlation of each pair of receiver outputs provides the amplitude and phase of the spatial coherence function for the baseline defined by the vector pointing from the first to the second receiver. These correlations are called the *visibilities*.

Ideal measurement model

To describe this mathematically, let us assume that there are J array elements called "antennas",[1] pointed at a field with Q point sources. Stack the sampled antenna signals for the k-th narrowband [6] frequency channel centered at frequency f_k into a $J \times 1$ vector $\mathbf{x}(n)$. For notational convenience, we will drop the dependence on frequency from the notation in most of the paper. Then we can model $\mathbf{x}(n)$ as

$$\mathbf{x}(n) \quad = \quad \sum_{q=1}^{Q} \mathbf{a}_q(n) s_q(n) + \mathbf{n}(n) \qquad (1)$$

where $s_q(n)$ is the signal from the q-th source at time sample n and frequency f_k, $\mathbf{a}_q(n)$ is the array response vector for this source, and $\mathbf{n}(n)$ is the noise sample vector. $s_q(n)$ and $\mathbf{n}(n)$ are baseband complex envelope representations of zero mean wide sense stationary white Gaussian random processes sampled at the Nyquist rate.

Due to Earth rotation the geometrical delay component of $\mathbf{a}_q(n)$ changes slowly with time, which is a critical feature exploited in synthesis imaging. Let N be the number of time samples in a short term integration (STI) interval. We assume that $\mathbf{a}_q(n)$ is (relatively) constant over such an interval, so that, for the m-th interval, $\mathbf{x}(n)$ is wide sense stationary over $(m-1)N \leq n \leq mN - 1$. A single STI autocovariance is defined as

$$\mathbf{R}_m = E\{\mathbf{x}(n)\,\mathbf{x}^H(n)\} = \mathbf{A}_m \mathbf{\Sigma}_s \mathbf{A}_m^H + \mathbf{\Sigma}_n, \qquad (2)$$

[1] As discussed in Sec. III, each element may be a phased array itself!

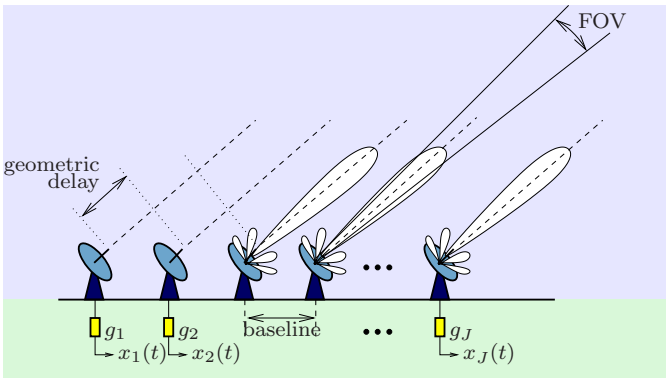

Fig. 3. Schematic overview of a radio interferometer.

where $\mathbf{R}_m$ has size $J \times J$,

$$\begin{aligned} \mathbf{A}_m &= \left[\mathbf{a}_1((m-1)N), \cdots, \mathbf{a}_Q((m-1)N)\right] \\ \mathbf{\Sigma}_s &= \mathrm{diag}\{[\sigma_1^2, \cdots, \sigma_Q^2]\} \\ \mathbf{\Sigma}_n &= E\{\mathbf{n}(n)\,\mathbf{n}^H(n)\} \;=\; \mathrm{diag}\{[\sigma_{n,1}^2, \cdots, \sigma_{n,J}^2]\}. \end{aligned}$$

Here, σ_q^2 is the variance of the q-th source. Noise is assumed to be independent but not evenly distributed across the array, and the noise variances $\sigma_{n,j}^2$ are unknown. With some abuse of notation, the subscript n in $\mathbf{\Sigma}_n$ and $\boldsymbol{\sigma}_{n,j}$ indicates "noise".

Each matrix element of $(\mathbf{R}_m)_{ij}$ represents the interferometric correlation along the baseline vector between the antennas i and j in the array. The corresponding short term integration sample covariance estimate is

$$\hat{\mathbf{R}}_m = \frac{1}{N} \sum_{n=(m-1)N}^{mN-1} \mathbf{x}(n)\mathbf{x}^H(n)\,,$$

and this is what the interferometer measures for subsequent processing. In practical instruments, the short-term integration interval is often in the order of 1 to 30 seconds, the total observation can span up to 12 hours, and the number of frequency bins is highly design-dependent ranging in order of magnitude from 10 to 10^5.

Under ideal circumstances, the array response matrix $\mathbf{A}_m$ is equal to a phase matrix $\mathbf{K}_m$ due entirely to the geometrical delays associated with the array and source geometry, and accurately known, at least for the calibration sources. The columns of $\mathbf{K}_m$, denoted by $\mathbf{k}_{m,q}$ $(q = 1, \cdots, Q)$, are often called the "Fourier kernel" and are given by

$$\begin{aligned} \mathbf{k}_{m,q} &= \exp\{\mathrm{j}\frac{2\pi f_k}{c}\mathbf{Z}^T\mathbf{p}_{m,q}\} \\ \mathbf{Z} &= \left[\mathbf{z}_1^T, \cdots, \mathbf{z}_J^T\right]^T, \end{aligned}$$

where c is the speed of light, $\mathbf{z}_j$ is the position column vector for the j-th array element, and $\mathbf{p}_{m,q}$ is a unit length vector pointing in the direction of source q during STI snapshot m.

Image formation

Ignoring the additive noise, the *measurement equation* (2), in its simplest form, can be written as

$$(\mathbf{R}_m)_{ij} = \sum_{q=1}^{Q} I(\mathbf{p}_q)\, e^{-\mathrm{j}\,(\mathbf{z}_i - \mathbf{z}_j)^T \mathbf{p}_{m,q}}$$

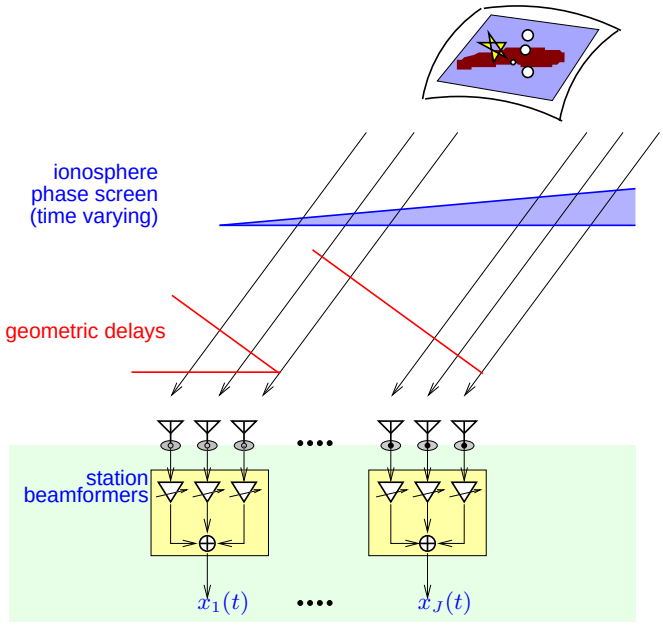

Fig. 4. A radio interferometer where stations consisting of phased array elements replace telescope dishes. The ionosphere adds phase delays to the signal paths. If the ionospheric electron density has the form of a *wedge*, it will simply shift the apparent positions of all sources.

where $(\mathbf{R}_m)_{ij}$ is the measured correlation between antennas i and j at STI interval m, $I(\cdot)$ is the brightness image (*map)* of interest, and $\mathbf{p}_q$ is the unit direction vector of the q-th source at a fixed reference time. It describes the relation between the observed visibilities and the desired source brightness distribution (intensities), and it has the form of a Fourier transform; it is known in radio astronomy as the Van Cittert-Zernike theorem [4], [7]. Image formation (*map making*) is essentially the inversion of this relation. Unfortunately, we have only a finite set of observations, therefore we can only obtain a *dirty image*:

$$\begin{aligned} I_D(\mathbf{p}) &:= \sum_{i,j,m} (\mathbf{R}_m)_{ij}\, e^{\mathrm{j}\,(\mathbf{z}_i - \mathbf{z}_j)^T \mathbf{p}} \\ &= \sum_{q} I(\mathbf{p}_q)\; B(\mathbf{p} - \mathbf{p}_q) \end{aligned}$$

where $\mathbf{p}$ corresponds to a pixel in the image, and where the *dirty beam*, also referred to as synthesized beam or point spread function (psf), is given by

$$B(\mathbf{p} - \mathbf{p}_q) := \sum_{i,j,m} e^{\mathrm{j}\,(\mathbf{z}_i - \mathbf{z}_j)^T (\mathbf{p} - \mathbf{p}_{m,q})}\,.$$

$I_D(\mathbf{p})$ is the desired image convolved with the dirty beam, essentially a non-ideal point spread function due to the finite sample effect. Every point source excites a beam $B(\cdot)$ centered at its location $\mathbf{p}_q$. *Deconvolution* is the process of recovering $I(\cdot)$ from $I_D(\cdot)$ using knowledge of the dirty beam. A standard algorithm for doing this is CLEAN [8]. The autocorrelations are often not used in the image formation process to reduce the impact of errors in the calibration of the additive noise on the resulting image. More details are shown in [9] and in the companion paper [5].

Non-ideal measurements

Although the previous equations suggest that it is rather straightforward to make an image from radio interferometer data, there are several effects that make matters more complicated:

- *Receiver element complex gain variations.* Astronomical signals are very weak, and radio telescopes therefore need to be very sensitive. This sensitivity is inversely proportional to the (thermal) noise. This dictates the use of low-noise amplifiers, which are sometimes even cryogenically cooled. Variations in environmental conditions of the receiver chain, such as temperature, cause amplitude and phase changes in the receiver response. Signals must also be propagated over long distances to a central processing facility and, depending on where digitization occurs, there can be significant phase and gain variations over time along these paths.
- *Instrumental response.* The sensitivity pattern of the individual elements, the *primary beam*, of an interferometer will never be perfect. Although it is steered towards the source of interest, the sensitivity in other directions (the *side lobe response*) on the sky will not be zero. This poses a challenge in the observation of very weak sources which may be hampered by signals from strong sources that are received via the side lobes, but are still competing with the signal of interest. The algorithms correcting for the instrumental response assume that the sensitivity pattern is known. This may not be true with the desired accuracy if the array is not yet calibrated.
- *Propagation effects.* Ionospheric and tropospheric turbulence cause time-varying refraction and diffraction, which has a profound effect on the propagation of radio waves. As illustrated in Fig. 4, in the simplest cases this leads to a shift in the apparent position of the sources. More generally, this leads to image distortions that are comparable to the distortions one sees when looking at ceiling lights from the bottom of a swimming pool.

In practice, $\mathbf{A}_m$ in (2) is thus corrupted by a complex gain matrix $\mathbf{G}_m$ which includes both source direction dependent perturbations and electronic instrumentation gain errors. It is the objective of calibration to estimate this matrix and track its changes over the duration of the observation. Some corrections (e.g., the complex antenna gain variations) can be applied directly to the measured correlation data, whereas other corrections (e.g., the propagation conditions) are direction dependent and are incorporated in the subsequent imaging algorithms. Very often, the estimation of the calibration parameters is done in an iterative loop that acts on the correlation (visibility) data and image data in turn, e.g., the self-calibration (SelfCal) algorithm [10], [11] discussed in more detail later in this paper.

III. Telescope architectures

The physical model underlying the array calibration depends on the instrument architecture. This architecture also determines the capabilities of the telescope and may therefore have a profound effect on the calibration strategy, as we will see later on.

The Westerbork Synthesis Radio Telescope (WSRT) and the Very Large Array (VLA) have been the work horses of radio astronomy since the 1970s. Both telescopes are arrays of 25 m dishes. The size of a dish determines its beamwidth, or *Field of View* (FOV) at a given wavelength, and hence the size of the resulting image, while the spatial extent of the array determines the resolution within the FOV. The illumination pattern of the feed on each dish determines its sensitivity pattern, which is commonly referred to as the primary beam. These telescopes can also form an instantaneous beam within this primary by coherent addition of the telescope signals (beamforming). This beam is called the array beam. Visibilities are measured by correlating the telescope signals. The baseline vectors on which the visibility function is observed during a full observation describe a synthesized aperture. The sampling within this aperture determines the sensitivity pattern of the synthesis observation, which is referred to as the synthesized beam or point spread function (psf) and corresponds to the dirty beam in the previous section. We thus have a beam hierarchy from the primary beam, which has a relatively large FOV (degrees) and relatively low sensitivity, via the instantaneously formed array beam to the point spread function, which has a small FOV (arcseconds) and a high sensitivity.

The WSRT and the VLA have their optimum sensitivity at frequencies of 1 to a few GHz. At lower frequencies, several things change. There are many more strong sources (e.g. synchrotron emission power is proportional to wavelength), thus even sources far outside the main beam of the psf may show their effect due to non-ideal spatial sampling. At low frequencies, the ionosphere is also much more variable (the phase delays are proportional to wavelength). Observations at these frequencies are therefore more challenging and require considerable processing power for proper calibration. High dynamic range imaging at these frequencies has therefore only recently been considered.

In the Low Frequency Array (LOFAR) [12], [13], which is currently being built in The Netherlands, the dishes are replaced by *stations*, each consisting of many small antennas distributed over an area of about 100×100 meter. Some stations are very closely spaced, others are placed up to several 100 km away from the core. A station is a phased array of receiving elements with its own beamformer. The stations are steered electronically instead of mechanically, which allows them to respond quickly to transient phenomena. The receiving elements can either be individual antennas (dipoles), or *compound elements* (tiles) consisting of multiple antennas whose signals are combined using an analog beamformer. This system concept introduces two additional levels in the beam hierarchy: the compound (tile) beam and the station beam. The complete hierarchy of beam patterns is illustrated in Fig. 5. The Murchison Widefield Array (MWA) has a similar design and purpose as LOFAR, but is placed in the outback of Western Australia and has a maximum baseline length of about 3 km. [14].

At first sight there is not much difference between the calibration of an array of stations (or dishes) and the calibration

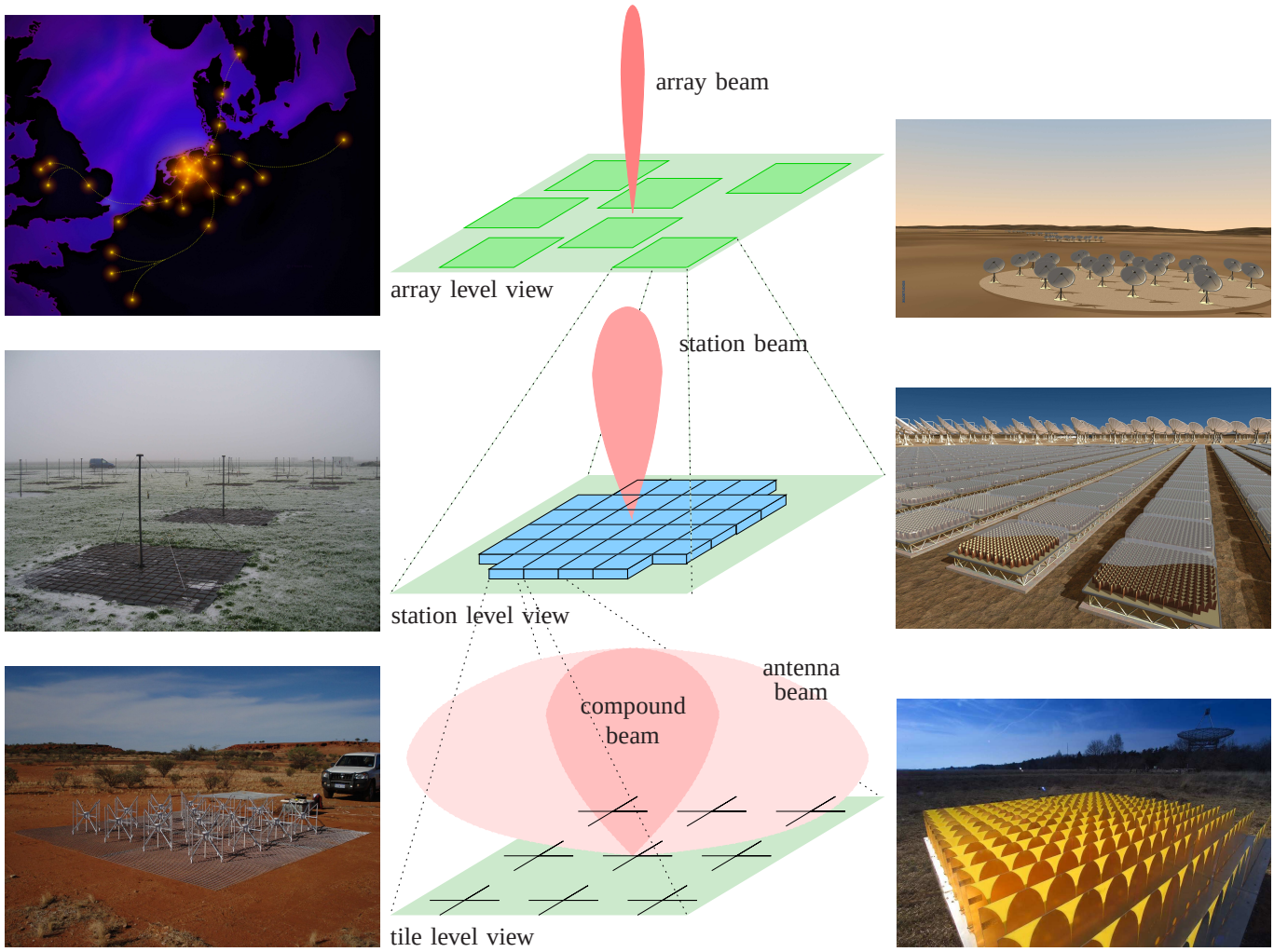

Fig. 5. *(Center column)* (d) The beamforming hierarchy with the array beam produced by an array of stations at the top and the antenna beam at the bottom. Subsequent levels in the hierarchy have beams that are narrower and more sensitive. *(Left column)* (a) the corresponding concept layout of LOFAR, (b) a LOFAR low band antenna station and (c) a MWA tile. *(Right column)* (e) a concept for SKA consisting of an array of stations, each with small dishes, (f) a concept for the SKA core station, and (g) a SKA demonstrator tile consisting of Vivaldi antennas.

of a station itself, but there are some subtle differences. A station only contains short baselines (~ 100 m), which implies that it provides a much lower resolution than an array, while its constituents provide a much wider FOV. As we will see in the next section, this implies that the calibration becomes more challenging due to direction dependent effects. Another challenging aspect stems from the enhanced flexibility of electronic beamforming: this may result in a less stable beam than a beam that is produced mechanically with a reflector dish. Finally, the output of a station beamformer is insufficient for calibration: for this purpose the station should also provide the correlation data among individual elements, even if these are not used at higher levels in the hierarchy.

A compound element (tile) can also be exploited as *focal plane array* (FPA). In this case, the array is placed in the focal plane of a dish. This allows to optimize the illumination of the dish, as it effectively defines a spatial taper over the aperture of the dish that can be used to create lower spatial side lobes. An FPA can also improve the FOV of the dish by providing multiple beams (off-axis) on the sky. In this case, the primary beam is the sensitivity pattern produced if the dish is illuminated by only a single antenna of the compound element. The compound beam is the electronically formed beam produced by illuminating the dish by the FPA. The FPA concept is currently under study in The Netherlands [15], United States [16], [17] and Australia [18] as part of the technology road map towards the Square Kilometer Array (SKA) [19].

SKA is a future telescope that is currently in the concept phase. It is a wide band instrument that will cover the frequency range from 70 MHz to above 25 GHz. Apart from cost the design is driven by a trade-off between sensitivity and survey speed: the speed at which the complete sky can be observed. To enable wide band operation, it will probably use a mix of receiver technologies:

- *Dishes with wide-band single pixel feeds.* At the highest frequencies this gives the highest sensitivity. Since this concept provides a very stable beam it is well suited for high fidelity imaging.
- *Dishes with focal plane arrays.* At intermediate frequen-

cies FPAs can be used to enlarge the FOV of a single dish in a cost effective way.

- *Aperture arrays.* At low frequencies, it is easier to obtain a large collecting area, hence sensitivity, by using dipoles instead of dishes. Aperture arrays have the additional advantage of being very flexible: by duplicating the receiver chains one can have multiple independent beams on the sky, bandwidth can be traded against the number of beams on the sky, and electronic beamforming provides a quick response time to transient events.

The configuration of SKA is still under study. Current concepts include a dense core that contains, e.g., half of all receivers within a diameter of 5 km, stations consisting of aperture arrays out to a maximal baseline of 180 km, and dishes out to a maximal baseline of 3000 km.

Notation

$\otimes$	Kronecker product
$\circ$	Khatri-Rao (columnwise Kronecker) product
$\odot$	Schur (entry-wise) matrix product
$\oslash$	entry-wise matrix division
$(\cdot)^T$	transpose operator
$(\cdot)^H$	Hermitian (conjugate) transpose operator
$(\mathbf{A})^{\odot\beta}$	entry-wise power of a matrix
$\mathrm{vec}(\cdot)$	stacking of the columns of a matrix
$\mathrm{diag}(\cdot)$	diagonal matrix constructed from a vector
$\overline{a}$	complex conjugate of a
$\dagger$	Moore-Penrose pseudo-inverse

IV. Calibration scenarios

In the previous section, we introduced several telescope architectures, each with different characteristics, hierarchy, and parameterizations of the observed data model. This will lead to a wide variety of calibration requirements and approaches. Fortunately, it is possible to discuss this in a more structured manner by using only four different scenarios [20], each of which can be described by a distinct specialization of the measurement equation [21]. Each scenario considers the calibration of an array of elements with complex gain variations and spatially varying propagation effects. The scenarios compare the *array aperture* (the length of the largest baseline) to the *field of View* (FOV, the beamwidth of each individual array element) and the *isoplanatic patch size*, i.e., the scale at which the ionosphere/troposphere can be considered constant.

Scenario 1. As shown in Fig. 6 (top left), the receiving elements of the array have a small FOV and the maximum baseline is short. In this case, all receiving elements and all lines of sight within the FOV experience the same propagation conditions: the propagation effects do not distort the image. This scenario represents the case in which direction dependent effects do not play a significant role. The calibration routine can therefore focus completely on element based gain effects. Since the FOV is small, it is often possible to calibrate on a single strong source in the FOV, especially if the array elements can be steered to a nearby calibration source. Due to its simplicity, this scenario is often used to obtain a first order calibration for new instruments.

Scenario 2. In this scenario (Fig. 6, top right), we have a large array consisting of elements with a small FOV. Lines of sight from different elements towards the region of interest are subject to different propagation conditions, but the propagation conditions for all lines-of-sight within the FOV of an individual element are the same. The propagation effects can therefore be merged with the unknown receiver gains of each element, and the array can be calibrated under the same assumptions as in the first scenario. This scenario is valid for most of the interferometers built in the 1970s and 1980s, such as the WSRT and the VLA, and for VLBI observations.

Scenario 3. Fig. 6 (bottom left) depicts the third scenario in which the elements have a large FOV, but the array is small. This implies that all lines of sight go through the same propagation path, but that there may be considerable differences in propagation conditions towards distinct sources within the FOV. The ionosphere and troposphere thus impose a direction dependent gain effect that is the same for all elements. This scenario can also handle instrumental effects that are the same for all elements (e.g., irregular antenna beamshapes) and is therefore well suited for the situation of a compact array of identical elements such as the MWA and a single LOFAR or SKA station.

Scenario 4. As shown in the bottom right panel of Fig. 6, the elements have a large FOV and the array has a number of long baselines. The lines of sight towards each source may experience propagation conditions that differ for different elements in the array. This implies that distinct complex gain corrections may be required for each source and each receiving element. Calibration is not possible without further assumptions on stationarity over space, time and/or frequency. This is the most general scenario, and valid for future telescopes such as LOFAR, SKA and ALMA.

V. Array calibration

Scenario 1

In scenario 1, the field of view (FOV) of each array element (dish) is small and it is reasonable to assume that there is only a single calibrator source within the beam. Often, the beam will even have to slightly point away from the field of interest to "catch" a nearby strong calibrator source. The calibrator should be unresolved, i.e., appear as a point source, as opposed to the extended structure visible in Fig. 1.

We will assume that the STI sample covariance matrices $\widehat{\mathbf{R}}_m$ are calibrated independently and omit the subscript m for notational convenience. Continuity over many STIs needs to be exploited under scenario 4 and will thus be discussed later. The data model (measurement equation) under scenario 1 is given by

$$\mathbf{R} = \mathbf{G}\mathbf{K}\mathbf{\Sigma}_s\mathbf{K}^H\mathbf{G}^H \; + \; \mathbf{\Sigma}_n \tag{3}$$

where $\mathbf{G} = \mathrm{diag}(\mathbf{g})$ is a diagonal matrix. For a single calibrator source, $\mathbf{K}$ has only a single column representing the geometric phase delays of the array towards the source, and $\mathbf{\Sigma}_s = \sigma_s^2$ is a scalar with the source power. Both the

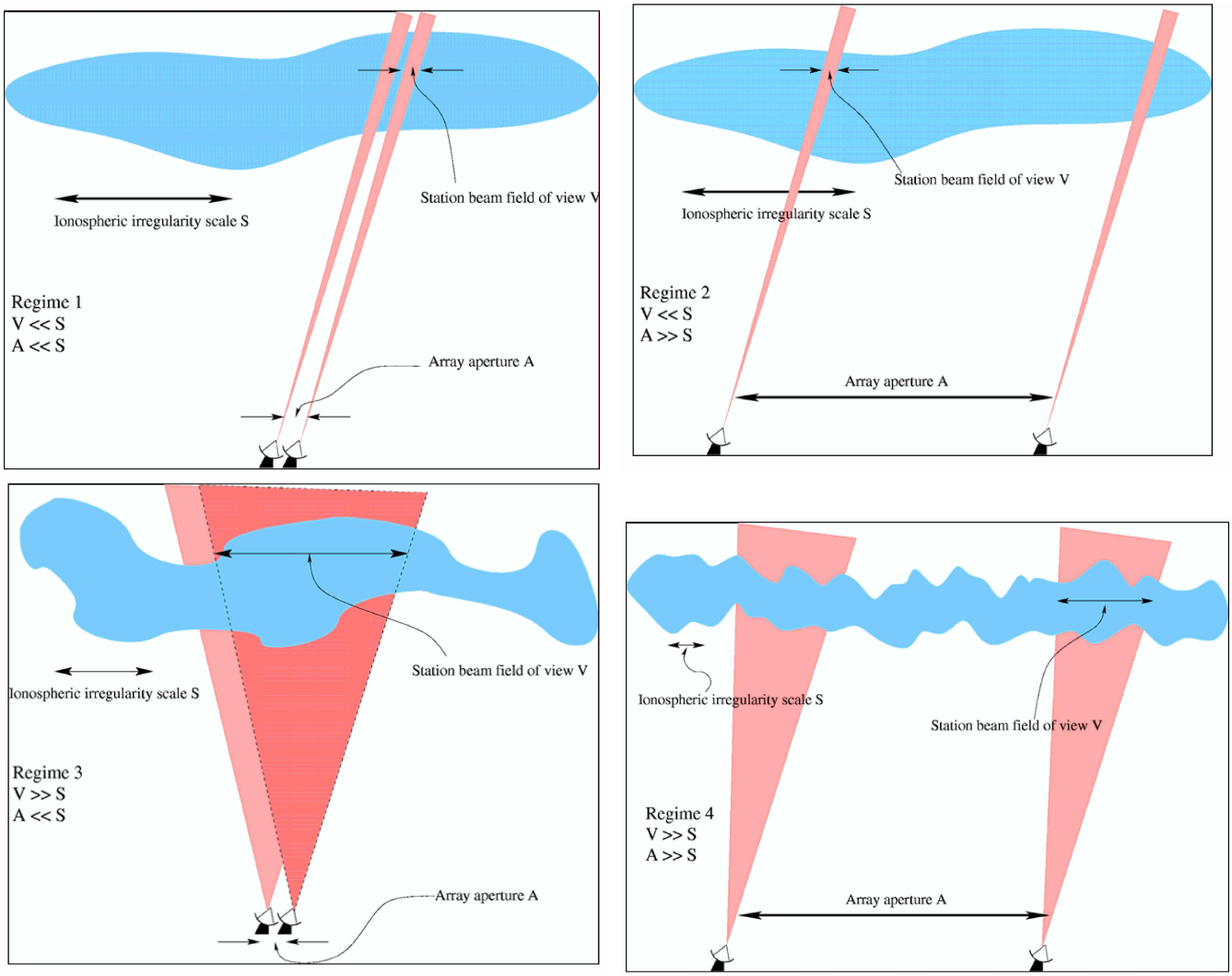

Fig. 6. Calibration scenarios 1 through 4 (top left to bottom right) as defined by Lonsdale [20]

direction of the source and its power are known from tables. Thus, in essence the problem simplifies to

$$\mathbf{R} \;=\; \mathbf{g}\mathbf{g}^H \;+\; \mathbf{\Sigma}_n$$

This is recognized as a "rank-1 factor analysis" model in multivariate analysis theory [22], [23]. Given $\widehat{\mathbf{R}}$, we can solve for $\mathbf{g}$ and $\mathbf{\Sigma}_n$ in several ways [24]–[26]. E.g., any submatrix away from the diagonal is only dependent on $\mathbf{g}$ and is rank 1: this allows direct estimation of $\mathbf{g}$. In the more general case described by (3), multiple calibrators may be simultaneously present. The required multi-source calibration is discussed in, e.q., [27]–[30].

Scenario 2

In this scenario, the ionospheric or tropospheric phases are different for each array element, but the field of view is narrow, and it is possible to assign the unknown ionospheric or tropospheric phases to the individual antennas. Thus, the problem reduces to that of Scenario 1, and the same calibration solution applies.

Scenario 3

This scenario is relevant for sufficiently compact arrays, e.g., the calibration of a SKA or LOFAR station or an array with a relatively small physical extend like the MWA. The phase and gain of the station beam FOV is direction dependent but the array elements see the same ionosphere. It is possible to make a coherent image, but sources may have shifted to different locations.

Since the FOV is large, several calibrator sources (say Q) will be visible. The model given by (3) for scenario 1 can be extended to include unknown source dependent complex gains,

$$\mathbf{R} = (\mathbf{G}_1\mathbf{K}\mathbf{G}_2)\mathbf{\Sigma}_s(\mathbf{G}_1\mathbf{K}\mathbf{G}_2)^H \;+\; \mathbf{\Sigma}_n\,,$$

where $\mathbf{G}_1 = \mathrm{diag}(\mathbf{g}_1)$ represents the antenna gain, and $\mathbf{G}_2 = \mathrm{diag}(\mathbf{g}_2)$ the source dependent complex gains, which describe the antenna beam shape and the propagation conditions. In this model, we can merge the unknown $\mathbf{G}_2$ with $\mathbf{\Sigma}_s$ to obtain a single unknown diagonal source matrix $\mathbf{\Sigma} = \mathbf{G}_2\mathbf{\Sigma}_s\mathbf{G}_2^H$, i.e.,

$$\mathbf{R} = \mathbf{G}\mathbf{K}\mathbf{\Sigma}\mathbf{K}^H\mathbf{G}^H \;+\; \mathbf{\Sigma}_n$$

Ionospheric calibration based on a statistical model

Assume for simplicity a single calibration source at zenith. The data model is

$$\mathbf{R} = \mathbf{a}\mathbf{a}^H\sigma_s^2 + \sigma_n^2\mathbf{I}$$

$\mathbf{a}$ is the spatial signature of the source at frequency f_k, as caused (only) by the ionosphere, and given by

$$\mathbf{a} = \exp(\mathrm{j}\boldsymbol{\phi})\,, \qquad \boldsymbol{\phi} = C\boldsymbol{\tau} f_k^{-1}$$

where $\boldsymbol{\phi}$ is a vector with J entries representing the ionospheric phases at each station, vector $\boldsymbol{\tau}$ contains the Total Electron Content (TEC) seen by each station, and C is a constant. The TEC is the integral of the electron density along the line of sight, and is directly related to a propagation delay.

The ionosphere is often modeled as a turbulent slab of diffracting medium. Assuming a single layer and a pure Kolmogorov turbulence process, the covariance for $\boldsymbol{\tau}$ is modeled by a power law of the form

$$\mathbf{C}_\tau = \mathbf{I} - \alpha(\mathbf{D})^{\odot\beta}$$

with unknown parameters α and β (theoretically, $\beta = 5/3$ but measured values show that deviations are possible). The matrix $\mathbf{D}$ contains the pairwise distances between all antennas, and is known.

Write the model as

$$\mathrm{vec}(\mathbf{R}) = (\bar{\mathbf{a}} \otimes \mathbf{a})\sigma_s^2 + \mathrm{vec}(\mathbf{I})\sigma_n^2$$

The observed covariance matrix is $\mathrm{vec}(\hat{\mathbf{R}}) = \mathrm{vec}(\mathbf{R}(\boldsymbol{\tau})) + \mathbf{w}$, where the observation noise $\mathbf{w}$ has covariance $\mathbf{C}_\mathbf{w} = \frac{1}{N}(\mathbf{R}^T \otimes \mathbf{R})$. At this point, we could estimate $\boldsymbol{\tau}$ by a Least Squares model matching. However, we have a priori knowledge on the parameters $\boldsymbol{\tau}$, i.e., the covariance $\mathbf{C}_\tau$. The maximum a posteriori (MAP) estimator exploits this knowledge, and leads to

$$\hat{\boldsymbol{\tau}} = \arg\min_{\boldsymbol{\tau}} \|\mathbf{C}_\mathbf{w}^{-\frac{1}{2}}\,\mathrm{vec}(\hat{\mathbf{R}} - \mathbf{R}(\boldsymbol{\tau}))\|^2 \;+\; \|\mathbf{C}_\tau^{-\frac{1}{2}}\boldsymbol{\tau}\|^2\,.$$

This is solved as a nonlinear least squares problem (α and β are estimated as well).

The dimensionality can be reduced by introducing $\boldsymbol{\tau} = \mathbf{U}\boldsymbol{\theta}$, where $\mathbf{U}$ contains a reduced set of basis vectors. These can be

- Data independent, e.g., simple polynomials, or Zernike polynomials [31],
- Data dependent (Karhunen-Loeve), based on an eigenvalue decomposition of $\mathbf{C}_\tau$: $\mathbf{C}_\tau \approx \mathbf{U}\boldsymbol{\Lambda}\mathbf{U}^H$. Only the dominant eigenvectors are retained.

Selection of the correct model order is often a tradeoff between reduced modeling error and increased estimation variance. Indeed, the simulation below indicates that the Least Squares estimator (with either a Zernike basis or a Karhunen-Loeve basis) has an optimal model order, beyond which the mean squared estimation error increases. The MAP estimator adds an additional term to the cost function that penalizes "weak" parameters and makes it robust to overmodeling. For more details, see [32]. The validity of the turbulence model is experimentally tested on VLA survey data in [33], [34].

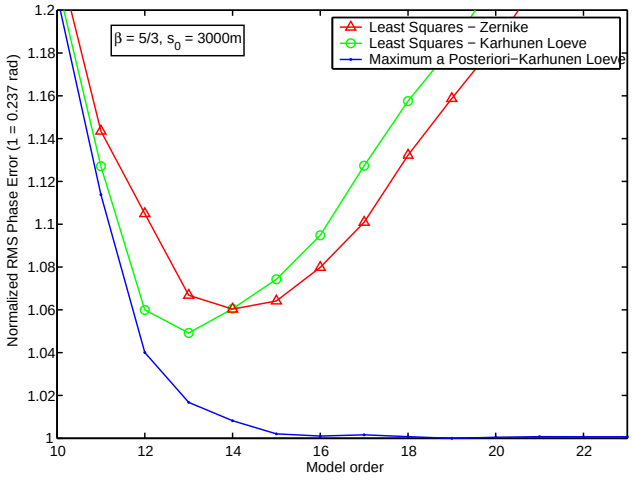

Estimation performance as function of model order selection

Given $\mathbf{R}$, the objective is to estimate $\mathbf{G}$, $\boldsymbol{\Sigma}$ and $\boldsymbol{\Sigma}_n$. Here, $\mathbf{K}$ is known as we know the source locations. If there is significant refraction, each viewing direction may pass through a different phase wedge, causing direction dependent motion of sources (but no further deformation). In that case, we will also have to include a parametric model for $\mathbf{K}$ and solve for the source directions (DOA estimation). This scenario is treated in, e.g., [30], [35].

The most straightforward algorithms to solve for the unknowns are based on alternating least squares. Assuming that a reasonably accurate starting point is available, we can solve $\mathbf{G}$, $\boldsymbol{\Sigma}$ and $\boldsymbol{\Sigma}_n$ in turn, keeping the other parameters fixed at their previous estimates [30]:

- *Solve for instrument gains:*

$$\begin{aligned}\hat{\mathbf{g}} &= \underset{\mathbf{g}}{\mathrm{argmin}} \|\hat{\mathbf{R}} - \mathbf{G}(\mathbf{K}\boldsymbol{\Sigma}\mathbf{K}^H)\mathbf{G}^H - \boldsymbol{\Sigma}_n\|^2 \\ &= \underset{\mathbf{g}}{\mathrm{argmin}} \|\mathrm{vec}(\hat{\mathbf{R}} - \boldsymbol{\Sigma}_n) + \\ &\quad -\mathrm{diag}(\mathrm{vec}(\mathbf{R}_0))(\overline{\mathbf{g}} \otimes \mathbf{g})\|^2\end{aligned}$$

where $\mathbf{R}_0 = \mathbf{K}\boldsymbol{\Sigma}\mathbf{K}^H$. This problem cannot be solved in closed form. Alternatively, we can first solve an unstructured problem: define $\mathbf{v} = \overline{\mathbf{g}} \otimes \mathbf{g}$ and solve

$$\hat{\mathbf{v}} = \mathrm{diag}(\mathrm{vec}(\mathbf{R}_0))^{-1}\mathrm{vec}(\hat{\mathbf{R}} - \boldsymbol{\Sigma}_n)$$

or equivalently

$$\widehat{\mathbf{g}\mathbf{g}^H} = (\hat{\mathbf{R}} - \boldsymbol{\Sigma}_n) \oslash \mathbf{R}_0.$$

where $\oslash$ denotes a pointwise division. After this, we can do a rank-1 approximation to find $\mathbf{g}$. The pointwise division can lead to noise enhancement; this is remediated by only using the result as initial estimate for, e.g., Gauss-Newton iteration [28] or by formulating a *weighted* least squares problem instead [26], [30].

- *Solve for source powers* $\boldsymbol{\sigma} = \mathrm{diag}(\boldsymbol{\Sigma})$*:*

$$\begin{aligned}\hat{\boldsymbol{\sigma}} &= \underset{\boldsymbol{\sigma}}{\mathrm{argmin}} \|\hat{\mathbf{R}} - \mathbf{G}\mathbf{K}\boldsymbol{\Sigma}\mathbf{K}^H\mathbf{G}^H - \boldsymbol{\Sigma}_n\|_F^2 \\ &= \underset{\boldsymbol{\sigma}}{\mathrm{argmin}} \|\mathrm{vec}((\hat{\mathbf{R}} - \boldsymbol{\Sigma}_n) - (\mathbf{G}\mathbf{K})\boldsymbol{\Sigma}(\mathbf{G}\mathbf{K})^H)\|^2 \\ &= \underset{\boldsymbol{\sigma}}{\mathrm{argmin}} \|\mathrm{vec}(\hat{\mathbf{R}} - \boldsymbol{\Sigma}_n) - \overline{(\mathbf{G}\mathbf{K})} \circ (\mathbf{G}\mathbf{K})\boldsymbol{\sigma}\|^2 \\ &= (\overline{\mathbf{G}\mathbf{K}} \circ \mathbf{G}\mathbf{K})^{\dagger}\mathrm{vec}(\hat{\mathbf{R}} - \boldsymbol{\Sigma}_n)\end{aligned}$$

- *Solve for noise powers* $\boldsymbol{\sigma}_n = \mathrm{diag}(\boldsymbol{\Sigma}_n)$*:*

$$\begin{aligned}\hat{\boldsymbol{\sigma}}_n &= \underset{\boldsymbol{\sigma}_n}{\mathrm{argmin}} \|\hat{\mathbf{R}} - \mathbf{G}\mathbf{K}\boldsymbol{\Sigma}\mathbf{K}^H\mathbf{G}^H - \boldsymbol{\Sigma}_n\|^2 \\ &= \mathrm{diag}(\hat{\mathbf{R}} - \mathbf{G}\mathbf{K}\boldsymbol{\Sigma}\mathbf{K}^H\mathbf{G}^H).\end{aligned}$$

A more optimal solution can be found by covariance matching estimation, which provides an asymptotically unbiased and statistically efficient solution [36]. However, there is no guarantee that this will hold for a weighted alternating least squares approach. Fortunately, the simulations in [30] suggest that it does for this particular problem, even if the method is augmented with weighted subspace fitting [37], [38].

The first step of this algorithm is closely related to the self-calibration (SelfCal) algorithm [10], [11] widely used in the radio astronomy literature, in particular for solving Scenario 1 and 2. In this algorithm, $\mathbf{R}_0$ is a reference model, obtained from the best known map at that point in the iteration.

An alternative implementation is Field-Based Calibration [39]. Assuming the instrumental gains have been corrected for, an image based on a short time interval is made. The apparent position shifts of the strongest sources are related to ionospheric phase gradients in the direction of each source. These "samples" of the ionosphere are interpolated to obtain a phase screen model over the entire field of view. This can be regarded as image plane calibration. The method is limited to the regime where the ionospheric phase can be described by a linear gradient over the array.

For the MWA currently a real time calibration method based on "peeling" is being investigated [40]. In this method of successive estimation and subtraction calibration parameters are obtained for the brightest source in the field. The source is then removed from the data, and the process is repeated for the next brightest source. This leads to a collection of samples of the ionosphere, to which a model phase screen can be fitted.

Scenario 4

This scenario is the most general case and should be applied to large arrays with a wide field of view such as LOFAR and SKA. In this case, each station beam sees a multitude of sources, each distorted by different ionospheric gains and phases. The data model for the resulting direction-dependent calibration problem is

$$\mathbf{R} = \mathbf{A}\boldsymbol{\Sigma}_s\mathbf{A}^H + \boldsymbol{\Sigma}_n \;=\; (\mathbf{G} \odot \mathbf{K})\boldsymbol{\Sigma}_s(\mathbf{G} \odot \mathbf{K})^H + \boldsymbol{\Sigma}_n\,,$$

where $\mathbf{G} = [\mathbf{g}_1, \cdots, \mathbf{g}_Q]$ is now a full matrix; $\boldsymbol{\Sigma}_s$ and $\mathbf{K}$ are known. $\mathbf{G}$ and $\boldsymbol{\Sigma}_n$ are unknown. Without making further assumptions, the solution is ambiguous: the gains are not identifiable.

This problem is discussed in [41] and studied in more detail in [42]. Possible assumptions that may lead to identifiability are:

- *Bootstrapping from a compact core.* The planned geometry of LOFAR and SKA includes a central core of closely packed stations. Under suitable conditions, these can be calibrated as under Scenario 3, giving a starting point for the calibration of the other stations.
- *Exploiting the different time and frequency scales.* Suppose we have a number of covariance observations $\mathbf{R}_{k,m}$, for different frequencies f_k and time intervals m. The matrix $\mathbf{K} = \mathbf{K}_{k,m}$ is varying over frequency and time, whereas the instrumental gains are relatively constant. This can be exploited to suppress contaminating sources by averaging over $\mathbf{K}_{k,m}$ while correcting the delays towards the calibrator sources.
- *Modeling the gain matrix* $\mathbf{G} = \mathbf{G}_{k,m}$. The gain matrix can be approximated by a low order polynomial model in k and m, leading to a reduction in the number of unknowns. As basis functions for the polynomials we can use the standard basis, or Zernike polynomials (often used in optics), or a Karhunen-Loeve basis derived from the predicted covariance matrix (see Box "Ionospheric calibration").
- *Successive estimation and subtraction or "peeling"*. In this method a distinction is made between the instrumental gains and ionospheric gains based on considerations such as temporal stability and frequency dependence. Sources are estimated and removed from the data in an iterative manner. This leads to a collection of samples to which a global model of the ionosphere or station beam can be fitted.

A complete calibration method that incorporates many of the above techniques was recently proposed in [43], and was successfully tested on a number of 74 MHz fields observed by the VLA. The behavior of this method at lower frequencies and / or on baselines longer than a few tens of kilometers still needs investigation.

VI. Compound element calibration

Compound elements are used in very large aperture arrays to keep the number of correlator inputs manageable, and as focal plane arrays to increase the FOV of dishes. In either case, each compound element produces a superposition of antenna signals, $\mathbf{x}(n)$, at its output port $y(n)$ during normal operation, i.e.,

$$y(n) = \mathbf{w}^H\mathbf{x}(n)$$

where $\mathbf{w}$ are the beamformer weights. Compound elements therefore require a separate calibration measurement before or after the observation, as only $y(n)$ is available and no antenna specific information can be derived from this superposition. Compound elements should thus be designed to be stable over the time scales of a typical observation.

Initial system characterization is often done in an anechoic chamber. In these measurements, the response $y(n)$ of the compound element to a test probe is recorded, while varying the beamformer $\mathbf{w}$ [44]. The measurements $y_1(n), y_2(n), \cdots, y_N(n)$ are stacked in a vector $\mathbf{y}$ while the corresponding weights $\mathbf{w}_1, \mathbf{w}_2, \cdots, \mathbf{w}_N$ are stacked in a matrix $\mathbf{W}$. The complete series can be summarized as

$$\mathbf{y}(n) = \mathbf{W}^H \mathbf{G}\mathbf{k}s(n)$$

where $s(n)$ is the known input signal, $\mathbf{k}$ is the phase vector describing the geometrical delays due to the array and source geometry and $\mathbf{G} = \mathrm{diag}\,(\mathbf{g})$ contains the instrumental gains. The gains of the individual elements stacked in $\mathbf{g}$ are then easily derived. An attractive feature of this method is that it can also be used in the field using a stationary reference antenna [45].

Calibration of an aperture array of compound elements is discussed in the previous section. Regarding its use as a focal plane array in a dish, there are a number of differences, mostly because the dish projects an image of the sky within its FOV onto the FPA, whereas an aperture array measures the complex field distribution over the aperture itself.

The goal of FPA beamforming is to maximize the signal-to-noise ratio in an observation [16]. This involves a trade-off between maximizing the gain in the direction of the source and minimization of the total noise in the system. A very intuitive approach to maximize the gain towards the source is conjugate field matching. For this calibration method, the array response $\mathbf{a}_p$ is measured for a strong point source for each of the P compound beams that will be formed by the FPA. The weights of the p-th compound beam are chosen such that $\mathbf{w}_p = \mathbf{a}_p$. Since the dish forms an image of the point source on the FPA, most of the energy is concentrated on a few elements. Conjugate field matching thus assigns very high weights to a few elements and the noise of these elements will therefore dominate the noise in the observation. If one of these elements has a poor noise performance, conjugate field matching does not lead to the maximum signal-to-noise ratio in the observation. The measurement on a strong point source should therefore be augmented with a measurement on an empty sky to obtain the noise covariance matrix of the array. This step allows proper weighting of the receiver paths to optimize the signal-to-noise ratio of the actual observation. An excellent overview of FPA signal processing is provided in [17].

VII. Future challenges

Instruments like LOFAR and SKA will have an unprecedented sensitivity that is two orders of magnitude higher (in the final image) than current instruments can provide. The increased sensitivity and large spatial extent requires new calibration regimes, i.e., scenarios 3 and 4, which are dominated by direction dependent effects. Research in this area is ongoing. Although many ideas are being generated, only a limited number of new calibration approaches have actually been tested on real data. This is hardly surprising since only now the first of these new instruments are producing data. Processing real data will remain challenging and drive the research in this area of signal processing. Apart from the challenges discussed already throughout the text, some of the remaining challenges are as follows.

- *The sky.* Because of the long baselines that are part of the new instruments, many sources which appear point-like to existing instruments, will be resolved. This means that they cannot be treated as point sources, but should be modeled as extended sources using, e.g., shapelets [46]. The new instruments will have wide frequency bands, so that the source structure may change over the observing band. For these reasons the source models will have to be more complicated than currently assumed. At the same time, due to the increased sensitivity, many more sources will be detected and will have to be processed. This will not only affect the calibration of the instruments, but also the imaging and deconvolution.
  Because of their high sensitivity the new instruments are capable of detecting very weak sources, but they will have to do so in the presence of all the strong sources already known. Some of those strong sources may not even be in the FOV, but may enter through the primary beam side lobes.
- *The instrument.* Both aperture arrays and dishes with FPAs have primary beams that are less stable than single pixel primary beams from dishes. The primary beam is time dependent (if it is not fixed on the sky) and varies with frequency and over the different stations or FPA systems. These beam pattern variations have a negative impact on the achievable image quality. Calibrating for these beams is a real challenge, as is the correction for such beams during imaging.
- *The atmosphere.* For low frequency instruments, ionospheric calibration is a significant challenge. Current algorithms have been shown to work for baselines up to a few tens of kilometers and frequencies as low as 74 MHz. However, for baselines of a few hundreds up to a few thousands of kilometers and frequencies down to, say, 10 MHz these algorithms may not be valid.
- *Polarization purity.* Calibration and imaging have to take the full polarization of the signal into account. The primary beam of an instrument introduces instrumental polarization due to the reception properties of the feeds. If the feeds do not track the rotation of the sky, as is the case in any radio telescope that does not have an equatorial mount, the instrumental polarization varies over the observation. The ionosphere alters the polarization of the incoming electromagnetic waves as well due to Faraday rotation. These effects require calibration and correction with high accuracy.
- *The large number of elements.* Classical radio telescopes have at most a few tens of receivers (WSRT has 14 dishes and the VLA has 27). Instruments like LOFAR, MWA and EMBRACE will have about 10^4 receiving elements while SKA is envisaged to have over 10^6 signal paths. The corresponding increase in data volumes will require sophisticated distributed signal processing schemes and

algorithms that can run on suitable high performance computing hardware.

- *Equations and unknowns.* It is clear that in order to deal with these challenges more complicated models are needed, which in turn contain more unknowns that need to be extracted from the data. The increase in the number of stations will yield more equations, but this may not be enough. Modeling of the time-frequency dependence of parameters by a suitable set of basis functions will decrease the amount of unknowns that need fitting.
- *Interference mitigation.* The radio frequency spectrum is rather crowded, and it is expected that many observations will be contaminated by (weak or strong) RFI. Array signal processing techniques can be used to suppress interference, e.g., by active null steering or covariance matrix filtering [47], [48]. For LOFAR and SKA, no techniques have been proposed yet. Research from cognitive radio and compressive sensing may be very relevant for interference avoidance.

Finding suitable answers to these challenges will be of critical importance for the next generation of instruments.

ACKNOWLEDGMENTS

This work was supported in part by NWO-STW (The Netherlands) under grant number DTC.5893. The Netherlands Institute for Research in Astronomy (ASTRON) is an institute of the Netherlands Organization for Scientific Research (NWO).

Credits for photos and artists impressions: Karl Jansky's antenna, Fig. $2(a)$: National Radio Astronomy Observatory (NRAO, www.nrao.edu); Effelsberg, Fig. $2(b)$: Stefan Wijnholds; WSRT, Fig. $2(c)$: Netherlands Institute for Radio Astronomy (ASTRON, www.astron.nl); VLA, Fig. $2(d)$: NRAO (www.vla.nrao.edu); ALMA, Fig. $2(e)$: ALMA observatory (www.almaobservatory.org); concept layout of LOFAR, Fig. $5\ (a)$: ASTRON; LOFAR low-band antennas, Fig. $5(b)$: Menno Norden; MWA tile, Fig. $5(c)$: MWA project (www.mwatelescope.org); artist impressions SKA, Figs. $5(e)$ and $5(f)$: SKA project (www.skatelescope.org); SKA demonstrator, Fig. $5(g)$: ASTRON.

AUTHORS

Stefan J. Wijnholds (wijnholds@astron.nl) was born in The Netherlands in 1978. He received the M.Sc. degree in Astronomy and the M.Eng. degree in Applied Physics (both cum laude) from the University of Groningen in 2003. After his graduation he joined the R&D department of ASTRON, the Netherlands Institute for Radio Astronomy, in Dwingeloo, The Netherlands, where he works with the system design and integration group on the development of the next generation of radio telescopes. Since 2006 he is also with TU Delft, The Netherlands, where he is pursuing a Ph.D. degree. His research interests lie in the area of array signal processing, specifically calibration and imaging.

Sebastiaan van der Tol (vdtol@strw.leidenuniv.nl) was born in The Netherlands in 1977. He received the M.Sc. degree in Electrical Engineering from TU Delft, The Netherlands, in 2004. Since January 2004 he has been a research assistant with the same institute, where he is pursuing a Ph.D. degree in Electrical Engineering. His current research interests include array signal processing and interference mitigation techniques for large phased array radio telescopes.

Ronald Nijboer (rnijboer@astron.nl) was born in The Netherlands in 1971. He received the Ph.D. degree in 1998 from the Vrije Universiteit, Amsterdam. From 1998 till 2004 he worked in the field of aeroacoustics with the National Aerospace Laboratory (NLR). In 2004 he started working for ASTRON, where at present he is leading the Computing group. His research interests include calibration and imaging algorithms.

Alle-Jan van der Veen (a.j.vanderveen@tudelft.nl) was born in The Netherlands in 1966. He received the Ph.D. degree (cum laude) from TU Delft in 1993. Throughout 1994, he was a postdoctoral scholar at Stanford University. At present, he is a Full Professor in Digital Signal Processing at TU Delft. He is the recipient of a 1994 and a 1997 IEEE Signal Processing Society (SPS) Young Author paper award, and was an Associate Editor for IEEE Tr. Signal Processing (1998–2001), chairman of IEEE SPS Signal Processing for Communications Technical Committee (2002-2004), Editor-in-Chief of IEEE Signal Processing Letters (2002-2005), Editor-in-Chief of IEEE Transactions on Signal Processing (2006-2008), and member-at-large of the Board of Governors of IEEE SPS (2006-2008). He is currently member of the IEEE SPS Awards Board and IEEE SPS Fellow Reference Committee. He is a Fellow of the IEEE.

REFERENCES

[1] Sloan digital sky survey home page. [Online]. Available: http://www.sdss.org

[2] G. Battaglia, F. Fraternali, T. Oosterloo and R. Sancisi, "HI study of the warped spiral galaxy NGC 5055: a disk/dark matter halo offset?" *Astronomy & Astrophysics*, vol. 447, pp. 49–62, Feb. 2006.

[3] M. Ryle, "A new radio interferometer and its application to the observation of weak stars," *Proc. Royal Society A*, vol. 211, pp. 351–375, 1952.

[4] A. R. Thompson, J. M. Moran and G. W. Swenson, *Interferometry and Synthesis in Radio Astronomy*, 2nd ed. New York: Wiley, 2001.

[5] R. Levanda and A. Leshem, "Image formation in radio astronomy," *IEEE Signal Processing Magazine*, vol. 27, no. 1, Jan. 2010.

[6] M. Zatman, "How narrow is narrowband," *IEE Proc. Radar, Sonar and Navig.*, vol. 145, no. 2, pp. 85–91, Apr. 1998.

[7] R. A. Perley, F. R. Schwab and A. H. Bridle, *Synthesis Imaging in Radio Astronomy*, ser. Astronomical Society of the Pacific Conference Series. BookCrafters Inc., 1994, vol. 6.

[8] J. A. Högbom, "Aperture synthesis with non-regular distribution of interferometer baselines," *Astronomy and Astrophysics Suppl.*, vol. 15, pp. 417–426, 1974.

[9] A. Leshem and A. J. van der Veen, "Radio-Astronomical Imaging in the Presence of Strong Radio Interference," *IEEE Transactions on Information Theory*, vol. 46, no. 5, pp. 1730–1747, Aug. 2000.

[10] T. J. Cornwell and P. N. Wilkinson, "A new method for making maps with unstable radio interferometers," *Mon. Not. R. Astron. Soc.*, vol. 196, pp. 1067–1086, 1981.

[11] T. J. Pearson and A. C. S. Readhead, "Image formation by self-calibration in radio astronomy," *Annual Rev. Astronomy and Astrophysics*, vol. 22, pp. 97–130, 1984.

[12] J. D. Bregman, "Concept design for a low frequency array," in *SPIE Proceedings Astronomical Telescopes and Instrumentation*, vol. 4015, 2000, pp. 19–33.

[13] M. de Vos, A. W. Gunst and R. Nijboer, "The LOFAR Telescope: System Architecture and Signal Processing," *Proceedings of the IEEE*, 2009, accepted for publication.

[14] C. Lonsdale, "The Murchison Widefield Array," in *Proceedings of the XXIXth General Assembly of the International Union of Radio Science (URSI GA)*, Chicago (Ill.), USA, 7-16 Aug. 2008.

[15] W. A. van Cappellen, J. G. bij de Vaate, M. V. Ivashina, L. Bakker and T. Oosterloo, "Focal Plane Arrays Evolve," in *Proceedings of the XXIXth General Assembly of the International Union of Radio Science (URSI GA)*, Chicago (Ill.), USA, 7-16 Aug. 2008.

[16] K. F. Warnick, and B. D. Jeffs, "Gain and Aperture Efficiency for a Reflector Antenna With an Arra y Feed," *IEEE Antennas and Wireless Propagation Letters*, vol. 5, no. 1, pp. 499–502, Dec. 2006.

[17] B. D. Jeffs, K. F. Warnick, J. Landon, D. Jones, J. R. Fisher and R. D. Norrod, "Signal Processing for Phased Array Feeds in Radio Astronomical Telescopes," *IEEE Journal of Selected Topics in Signal Processing*, vol. 2, no. 5, pp. 635–646, Oct. 2008.

[18] D. DeBoer, "Australian SKA Pathfinder," in *Proceedings of the XXIXth General Assembly of the International Union of Radio Science (URSI GA)*, Chicago (Ill.), USA, 7-16 Aug. 2008.

[19] P. J. Hall, "The Square Kilometer Array: an International Engineering Perspective," *Experimental Astronomy*, vol. 17, no. 1-3, pp. 5–16, 2004.

[20] C. Lonsdale, "Calibration approaches," MIT Haystack, Tech. Rep. LFD memo 015, Dec. 8, 2004.

[21] J. Hamaker, J. Bregman, and R. Sault, "Understanding radio polarimetry - I. Mathematical foundations," *Astronomy & Astrophysics Supplement Series*, vol. 117, pp. 137–147, May 1996.

[22] K. V. Mardia, J. T. Kent and J. M. Bibby, *Multivariate Analysis*. Academic Press, 1979.

[23] D. N. Lawley and A. E. Maxwell, *Factor Analysis as a Statistical Method*. Butterworth & Co, London, 1971.

[24] A. J. Boonstra and A. J. van der Veen, "Gain calibration methods for radio telescope arrays," *IEEE Trans. Signal Processing*, vol. 51, no. 1, pp. 25–38, Jan. 2003.

[25] A. J. Boonstra, S. J. Wijnholds, S. van der Tol and B. Jeffs, "Calibration, Sensitivity and RFI Mitigation Requirements for LOFAR," in *IEEE International Conference on Acoustics, Speech and Signal Processing (ICASSP)*, Philadelphia (Penn.), USA, 18-23 Mar. 2005.

[26] S. J. Wijnholds and A. J. Boonstra, "A Multisource Calibration Method for Phased Array Telescopes," in *Fourth IEEE Workshop on Sensor Array and Multi-channel Processing (SAM)*, Waltham (Mass.), USA, July 2006.

[27] J. Pierre and M. Kaveh, "Experimental Performance of Calibration and Direction Finding Algorithms," in *Proceedings Internation Conference on Acoustics, Speech and Signal Processing (ICASSP) '91*, vol. 2, Toronto (Canada), May 1991, pp. 1365–1368.

[28] D. R. Fuhrmann, "Estimation of Sensor Gain and Phase," *IEEE Trans. Signal Processing*, vol. 42, no. 1, pp. 77–87, Jan. 1994.

[29] B. P. Flanagan and K. L. Bell, "Array Self Calibration with Large Sensor Position Errors," *Signal Processing*, vol. 81, no. 10, pp. 2201–2214, Oct. 2001.

[30] S. J. Wijnholds and A. J. van der Veen, "Multisource Self-calibration for Sensor Arrays," *accepted, IEEE Tr. Signal Processing*, 2009.

[31] W. D. Cotton and J. J. Condon, "Calibration and imaging of 74 MHz data from the Very Large Array," in *XXVIIth General Assembly of the International Union of Radio Science (URSI)*, Maastricht (The Netherdlands), Aug. 2002.

[32] S. van der Tol and A. J. van der Veen, "Ionospheric calibration for the LOFAR radio telescope," in *Proc. IEEE Int. Symp. Signals, Circuits, Systems*. Iasi, RO: IEEE, July 2007.

[33] A. S. Cohen and H. J. A. Röttgering, "Probing fine-scale ionospheric structure with the Very Large Array Radio Telescope," *In preparation*, 2009.

[34] S. van der Tol, R. Sridharan, A. J. van der Veen, H. J. A. Röttgering and A. S. Cohen, "Verification of an ionospheric turbulence model by VLA 74 MHz data," *In preparation*, 2009.

[35] A. J. Weiss and B. Friedlander, "'Almost Blind' signal estimation using second order moments," *IEE Proceedings on Radar, Sonar and Navigation*, vol. 142, no. 5, pp. 213–217, Oct. 1995.

[36] B. Ottersten, P. Stoica and R. Roy, "Covariance Matching Estimation Techniques for Array Signal Proce ssing Applications," *Digital Signal Processing, A Review Journal*, vol. 8, pp. 185–210, July 1998.

[37] M. Viberg and B. Ottersten, "Sensor Array Processing Based on Subspace Fitting," *IEEE Trans. Signal Processing*, vol. 39, no. 5, pp. 1110–1121, May 1991.

[38] M. Viberg, B. Ottersten and T. Kailath, "Detection and Estimation in Sensor Arrays Using Weighted Subsp ace Fitting," *IEEE Trans. Signal Processing*, vol. 39, no. 11, pp. 2436–2448, Nov. 1991.

[39] W. D. Cotton, J. J. Condon, R. A. Perley, N. Kassim, J. Lazio, A. S. Cohen, W. Lane and W. C. Erickson, "Beyond the isoplanatic patch in the VLA Low-frequency Sky Survey," in *Proc. SPIE*, vol. 5489, Glasgow, June 2004, pp. 180–189.

[40] D. A. Mitchell, L. J. Greenhill, R. B. Wayth, R. J. Sault, C. J. Lonsdale, R. J. Cappallo, M. F. Morales and S. M. Ord, "Real-Time Calibration of the Murchison Widefield Array," *IEEE Journal of Selected Topics in Signal Processing*, vol. 2, no. 5, pp. 707–717, Oct. 2008.

[41] J. E. Noordam, "Generalized self-calibration for LOFAR," in *XXVIIth General Assembly of the International Union of Radio Science (URSI)*, Maastricht (The Netherlands), Aug. 2002, http://www.ursi.org/Proceedings/ProcGA02/papers/1087.pdf.

[42] S. van der Tol, B. D. Jeffs and A. J. van der Veen, "Self-Calibration for the LOFAR Radio Astronomical Array," *IEEE Transactions on Signal Processing*, vol. 55, no. 9, pp. 4497–4510, Sept. 2007.

[43] H. T. Intema, S. van der Tol, W. D. Cotton, A. S. Cohen, I. M. van Bemmel and H. J. A. Röttgering, "Ionospheric calibration of low frequency radio interferometric observations using the peeling scheme. I. Method description and first results," *Astronomy & Astrophysics (submitted)*, 2009.

[44] G. A. Hampson and A. B. Smolders, "A Fast and Accurate Scheme for Calibration of Active Phased Array Antennas," in *IEEE Antennas and Propagation Society International Symposium*, vol. 2, Orlando (Fl.), USA, 7-16 July 1999, pp. 1040–1043.

[45] S. J. Wijnholds, "Evaluation and Demonstration of THEP as a Radio Astronomical Observing Facility," Master's thesis, University of Groningen, 2003.

[46] A. Refreiger, "Shapelets - I. A method for image analysis," *Monthly Notices of the Royal Astronomical Society*, vol. 338, pp. 35–47, 2003.

[47] A. Leshem and A. J. van der Veen and A. J. Boonstra, "Multichannel interference mitigation techniques in radio astronomy," *Astrophysical Journal Supplements*, vol. 131, no. 1, pp. 355–374, Nov. 2000.

[48] A. J. van der Veen and A. Leshem and A. J. Boonstra, "Signal processing for radio astronomical arrays," in *IEEE workshop on Sensor Array and Multichannel*, Sitges (Spain), July 2004.